# Rapid short-pulse sequences enhance the spatiotemporal uniformity of acoustically-driven microbubble activity during flow conditions

Antonios N. Pouliopoulos, Caiqin Li

*Bioengineering Department, Imperial College London, London, SW7 2BP, United Kingdom*

Marc Tinguely, Valeria Garbin

*Chemical Engineering Department, Imperial College London, London, SW7 2AZ, United Kingdom*

Meng-Xing Tang and James J. Choi[a)]

*Bioengineering Department, Imperial College London, London, SW7 2BP, United Kingdom*

[a)] Author to whom correspondence should be addressed. Electronic mail: j.choi@imperial.ac.uk

Running title: Short pulses for uniform ultrasound therapy

Keywords: acoustic cavitation; ultrasound therapy; passive acoustic mapping; high-speed microscopy

**ABSTRACT**

Despite the promise of microbubble-mediated focused ultrasound therapies, *in vivo* findings have revealed over-treated and under-treated regions distributed throughout the focal volume. This poor distribution cannot be improved by conventional pulse shapes and sequences, due to their limited ability to control acoustic cavitation dynamics within the ultrasonic focus. We have designed a rapid short-pulse (RaSP) sequence which is comprised of short pulses separated by μs off-time intervals. Improved acoustic cavitation distribution was based on the hypothesis that microbubbles can freely move during the pulse off-times. Flowing SonoVue® microbubbles (flow velocity: 10mm/s) were sonicated with a 0.5 MHz focused ultrasound transducer using RaSP sequences (peak-rarefactional pressures: 146-900 kPa, pulse repetition frequency: 1.25 kHz, and pulse lengths: 5-50 cycles). We evaluated the distribution of cavitation activity using passive acoustic mapping. RaSP sequences generated uniform distributions within the focus in contrast to long pulses (50,000 cycles) that produced non-uniform distributions. Fast microbubble destruction occurred for long pulses, whereas microbubble activity was sustained for longer durations for shorter pulses. High-speed microscopy revealed increased mobility in the direction of flow during RaSP sonication. In conclusion, RaSP sequences produced spatiotemporally uniform cavitation distributions and could result in efficient therapies by spreading cavitation throughout the treatment area.

PACS numbers: 43.80.Gx, 43.80.Sh, 43.80.Ev

## I. INTRODUCTION

Acoustically-driven microbubble activity has been employed in a multitude of therapeutic applications to date (Coussios and Roy, 2008; Stride and Coussios, 2010), including targeted drug delivery (Ferrara et al., 2007), blood-brain barrier opening (Konofagou, 2012), sonoporation (Yu and Xu, 2014), and renal filtration (Deelman et al., 2010). In a typical ultrasonic therapy setting, focused ultrasound is generated outside the body and propagates deep into the tissues, to converge to a targeted region of interest. Although ultrasound alone can produce a desired bioeffect (Dalecki, 2004; Fischer et al., 2009), many ultrasound techniques are combined with pre-formed microbubbles that act as discrete sites of mechanical stress within the vasculature and allow for sub-focal volume localisation of mechanical effects.

Microbubbles are acoustically responsive particles with diameters between 1 and 5μm and are typically composed of a compressible gas core and a lipid or protein shell (Lindner, 2004). Due to their minute size, pre-formed systemically administered microbubbles can freely flow within the vascular compartment without extravasating from the vessel lumen. Their compressible core enables microbubbles to respond to ultrasound within the target area in a complex range of behaviours collectively known as acoustic cavitation (Apfel, 1997), which refers to the volumetric oscillations of a cavity due to compressional and rarefactional phases of a pressure wave. Due to their compressible gas core, which allows them to scatter ultrasound, microbubbles are widely used as ultrasound contrast agents in imaging applications (Cosgrove, 2006; Stride and Saffari, 2003) and, more recently, as palpation agents to derive the elasticity of tissues (Koruk et al., 2015). In ultrasound therapy, the acoustic cavitation activity of each microbubble is the source of both wanted and unwanted bioeffects, thus understanding and controlling its dynamics is vital to producing the sought therapeutic outcome.

Depending on the ultrasound field and exposure conditions, the microbubble population characteristics, and the local microenvironment, different microbubble dynamics can be produced. Acoustic cavitation is classified according to categories that describe the nature of radial oscillations: periodicity and dominant driving force (Church and Carstensen, 2001; Flynn, 1982). The periodicity of cavitation activity can be described as stable or transient, while the dominant driving force can be described as inertial and non-inertial (Apfel, 1997). In stable cavitation microbubbles radially oscillate in a periodic manner whereas in transient cavitation these oscillations cease to occur during sonication due to either bubble collapse, fragmentation (Chomas et al., 2001), or gas dissolution to the surrounding fluid (Borden and Longo, 2002). In inertial cavitation, an unstable expansion phase leads to a rapid collapse dominated by the inertia of the surrounding fluid whereas in non-inertial cavitation the ultrasound field dictates the dynamics of the microbubble volumetric changes. Different cavitation modes are not mutually exclusive and a mixture of these modes are often observed in microbubble cloud responses (Choi and Coussios, 2012; Flynn, 1982). Because the commercially available microbubbles are inherently polydisperse and the local microenvironment cannot be modified, control of microbubble dynamics can only be achieved by modifying the characteristics of the ultrasound pulse shape and sequence (Pouliopoulos et al., 2014).

The ultrasound pulse shape is typically defined by the center frequency, the peak rarefactional pressure, and the pulse length (number of ultrasound cycles). The ultrasound center frequency relative to the microbubble resonance frequency affects the radial oscillation magnitude (Helfield and Goertz, 2013; Marmottant et al., 2005). Therapeutic ultrasound center frequencies within the 0.25 - 2 MHz range are not uncommon to use and allow for deeper penetration and larger treatment volumes. However, the resonance frequencies of commercial microbubbles lie within the 2-5 MHz range (van der Meer et al., 2007), which

implies that most microbubbles are off-resonance in therapeutic applications. Acoustic pressure determines the amplitude of the microbubble radial oscillations and is a major factor that dictates the cavitation modes and concomitant bioeffects. By increasing the pressure, the microbubble cloud acoustic response shifts from stable non-inertial to transient inertial cavitation, i.e. nuclei collapse and fragment (Chomas et al., 2001). Long pulse lengths were shown to decrease the inertial cavitation threshold at the same pressure (Chen et al., 2003a; Gruber et al., 2014). Microbubble translational dynamics are also affected by the pulse length, with longer pulses leading to increased primary and secondary acoustic radiation force effects (Dayton et al., 2002; Palanchon et al., 2005). Therapeutic applications such as blood-brain barrier opening have been typically performed at pressures in the range 0.3-1 MPa and pulse lengths on the order of 10-100ms (Choi et al., 2007a; Hynynen et al., 2001; Tung et al., 2010). Cavitation responses can be monitored by analysing the spectrum of the acoustic emissions radiated by sonicated microbubbles. High magnitude stable non-inertial and low magnitude inertial cavitation are characterised by strong emissions at the sonication center frequency and its harmonics, while high magnitude inertial cavitation increases the level of broadband signal. These emissions have been used in real-time feedback-control systems, in order to achieve the desired mixture of cavitation responses at each pulse (Hockham et al., 2010; O'Reilly and Hynynen, 2012).

Although the pulse shape dictates the microbubble behaviour on the microsecond scale, the pulse sequence influences the number of times these dynamics occur and the location where they occur (Choi et al., 2011a, 2011b). By the end of a traditionally long therapeutic pulse (e.g., 10 ms), a large percentage of the microbubbles are either destroyed or modified, hence a pulse off-time on the order of seconds is required for the replenishment of the focal volume with fresh cavitation nuclei (Goertz et al., 2010). The total number of pulses or total treatment duration period determines the amount of cavitation events the target area is treated

by. Together, the ultrasound pulse shape and sequence produce a specific set of cavitation magnitudes, types, durations, and distributions within the focal volume (Choi and Coussios, 2012).

Conventional long-pulse and high-pressure therapeutic pulses with pulse repetition frequencies on the order of Hz have been successfully used to deliver drugs across the blood-brain barrier (Hynynen et al., 2001) or to dissolve blood clots (Holland et al., 2002). Higher efficacy (e.g., greater drug delivery doses across capillaries) is often achieved by using a stronger mode of cavitation (e.g., inertial cavitation), thus causing increased mechanical stress which produced a spot-like distribution of bioeffects (Stieger et al., 2007). However, higher pressures have also been associated with increased damage, such as erythrocyte extravasation and cellular necrosis (Baseri et al., 2010; Liu et al., 2008). Thus, there is a trade-off between efficacy and safety with adjusting pressures. At the tissue level, over-treated and under-treated areas can be observed (Choi et al., 2007b). *In vitro* studies have provided evidence that the basis of the poor uniformity of bioeffects is the inadequate distribution of the acoustic cavitation activity within the focal volume (Choi and Coussios, 2012). Microbubbles flowing into the focal volume and exposed to long-pulse, high-pressure sonication are destroyed within a few milliseconds. Fast microbubble destruction was shown to produce an upstream spatial bias in the total emitted energy, i.e. an accumulation of acoustic energy at the upstream part of the flow. Thus we sought an alternative pulse shape and sequence design to overcome the produced bias and improve efficacy without compromising safety. This can be achieved by spreading a safe mode of cavitation activity throughout the target area and maintaining it for the entire treatment period.

*In vivo* studies have reported that short-pulse sonication with short off-times on the order of μs has led to a significant improvement to the uniformity and magnitude of the drug permeability increase in blood-brain barrier disruption without any associated damage to the

brain tissue (Choi et al., 2011a, 2011b). This empirical observation has been recently complemented by *in vitro* indirect evidence suggesting that rapid short-pulse (RaSP) sequences can be used to extend the lifetime of flowing microbubbles within the focal volume (Pouliopoulos et al., 2014). Sonication with short pulse lengths and off-time intervals on the range of μs led to longer persistence of microbubble acoustic emissions and thus enhanced the spatiotemporal distribution of acoustic cavitation activity. However, this required the assumption that microbubbles move during the off-time periods. To date there has been no direct evidence of improved distribution using this new pulse shape and sequence design.

The aim of this study was to directly assess the spatiotemporal distribution of the acoustic activity of flowing microbubbles sonicated by RaSP sequences in comparison with conventional long pulse sequences. Passive acoustic mapping (PAM) has been previously used to determine the location of acoustic events both *in vitro* (Choi and Coussios, 2012; Gyöngy and Coussios, 2010a) and *in vivo* (Choi et al., 2014) and will be used here evaluate the efficacy of RaSP sequences. In order to resolve individual microbubbles within a small volume, we used high-speed optical microscopy. Our hypotheses were that short-pulse sonication leads to a more uniform distribution of acoustic cavitation activity than conventional long-pulse sonication and that PAM can be used to monitor and quantify acoustic cavitation activity distribution for the RaSP sequences.

## II. METHODS

### A. Experimental setup

#### 1. In vitro *flow apparatus*

Our *in vitro* flow experiments were conducted in a tank containing deionized and degassed water (Fig. 1(a)-1(b)). An arteriole-like silicon elastomer tube (inner diameter: 0.8

mm, outer diameter: 1.6 mm; Saint-Gobain Performance Plastics, Paris, France) was submerged into the tank and fixed at a horizontal position. SonoVue® microbubbles, which are routinely used in the clinical applications as an imaging contrast agent, were generated according to the manufacturer's instructions and diluted to the recommended clinical dose (50 μl of SonoVue® solution in 100ml of solution). To ensure uniform distribution of microbubbles during the entire experiment duration, the microbubble solution was placed in a beaker and continuously mixed with a magnetic stirrer (Jencons-VWR, East Grinstead, UK). A syringe pump (Instech, Plymouth Meeting, PA, USA) was used to withdraw the microbubble solution at a fluid velocity of 10 mm/s, on the same order of magnitude with physiologically relevant blood velocities (Tangelder et al., 1986).

A spherically-focused single-element 0.5 MHz ultrasound transducer (active diameter: 64 mm, f-number: 0.98, FWHM: 5.85 mm, focal length: 62.6 mm, part number: H-107; Sonic Concepts Inc., Bothell, WA, USA) was used to sonicate the flowing microbubbles. The transducer was driven by two function generators (33500B Series, Agilent technologies, Santa Clara, CA, USA), controlled with Matlab (The Mathworks, Natick, MA, USA) to emit the different pulse shapes and sequences. A 50dB power amplifier (Precision Acoustics Ltd, Dorchester, UK) was used to amplify the pulses, which were then applied to the ultrasonic transducer via an impedance matching box (Sonic Concepts Inc., Bothell, WA, USA). Before every experiment the tube was positioned within the focal volume that was defined earlier with a 0.2 mm diameter polyvinylidene fluoride (PVDF) needle hydrophone (Precision Acoustics Ltd, Dorchester, UK).

Acoustic emissions generated by sonicated microbubbles were passively captured with an ATL L7-4 linear array (center frequency: 5.2 MHz, number of elements: 128, aperture size: 38.4 mm, element spacing: 0.3 mm; Philips Healthcare, Guildford, Surrey, UK). The array was oriented so that its imaging plane was orthogonal to the therapeutic ultrasound

beam propagation direction and aligned with the tube's length (Fig. 1(a)-1(b)). A 128-channel Verasonics Vantage research platform (Verasonics Inc., Kirkland, WA, USA) was used for the alignment of the setup and the recording of radiofrequency (RF) acoustic signals. Using the PVDF hydrophone and conventional B-mode ultrasound imaging, we positioned the array in a way such that the center of the acoustic focus of the therapeutic transducer was close to the central elements of the linear array. A B-mode image was saved to allow for accurate depiction of the tube elevational position in the processed data. Verasonics acquisition was triggered by the function generator, while the acquisition duration and the repetition period were selected to be 150 μs and 800μs, respectively, so that the entire cavitation signal fitted within a frame (Fig. 2). An appropriate delay between emission and reception was chosen in every experiment, in order to account for the ultrasound time of flight and the software or hardware delays. All raw data were saved for off-line post-acquisition processing.

***2. Ultrasound parameters***

Our choice of ultrasound parameters was guided by previous results that showed an indirect improvement of the acoustic cavitation distribution *in vitro* (Pouliopoulos et al., 2014) and an enhanced induced bioeffect *in vivo* (Choi et al., 2011b). Briefly, we replaced a conventional 100-ms-long ultrasonic pulse, which is routinely used in ultrasound therapy applications (Choi et al., 2014), with a RaSP sequence (Pouliopoulos et al., 2014). In effect, we kept the sonication duration equal to 100ms but introduced short off-time periods on the order of μs, in order to facilitate microbubble movement between pulses and prolong the microbubble cloud lifetime. Following previously introduced terminology (Choi et al., 2011b; Pouliopoulos et al., 2014), we refer to the train of short pulses as a single burst. The pulse repetition frequency (PRF) and the pulse lengths (PL) within the burst were 1.25 kHz and on the order of tens of μs respectively (Fig. 2 and table I). The number of pulses emitted

was equivalent in each parametric set evaluated. As a result, the total energy emitted was lower for the shorter pulse lengths evaluated. By varying the PL one could modify the cavitation distribution within the focus. With a fluid velocity of 10 mm/s and a pulse repetition period of 800 μs, individual microbubbles would flow for approximately 8 μm between each pulse or 1 mm during an entire burst. When considering a microbubble population distributed across the therapeutic beam, sonication with RaSP sequences could allow for uniform treatment of the entire focal area (Pouliopoulos et al., 2014). To unravel the spatially- and temporally-resolved acoustic cavitation outcome of each distinct pulse sequence, we captured the radiated acoustic emissions using the linear array and processed the raw RF channel data using the PAM technique combined with robust Capon beamforming.

## B. Passive Acoustic Mapping

### *1. Reconstruction algorithm*

Microbubble-seeded acoustic cavitation activity within the sonicated focal area was mapped using a script to perform PAM written in Matlab. RF data was captured from each of the 128 elements of the ATL L7-4 array at a frame rate equal to the PRF of the rapid short-pulse sequence (i.e., 1.25 kHz), and consisted of 150 μs long data sets sampled at 20.8MHz, with each short pulse fitting within one acquisition frame (Fig. 2).

The idea of localising the source of sound and eliminating spatially-incoherent noise from other locations was reported for biomedical ultrasound applications by Gyöngy et al. (2008) and, using a similar method, by Salgaonkar et al. (2009). The PAM algorithm can estimate the acoustic cavitation source strength at a specific location as previously described (Gyöngy and Coussios, 2010a, 2010b; Gyöngy and Coviello, 2011). Assuming a single

acoustic event at location $\boldsymbol{r}$ with an acoustic strength of $q(\boldsymbol{r},t)$, the pressure generated at any location $\boldsymbol{r}'$ and at time $t$ will be:

$$p(\boldsymbol{r}',t)=\frac{q\left(t-|\boldsymbol{r}'-\boldsymbol{r}|/c\right)}{4\pi|\boldsymbol{r}'-\boldsymbol{r}|} \tag{1}$$

where $c$ is the speed of sound of water, set to 1497 m/s. Eq. (1) accounts for the spherical propagation of the acoustic wave and the time of arrival from the source to the observer. Inverting Eq. (1) enables an estimation of the acoustic source strength based on the acoustic pressures $\tilde{p}(\boldsymbol{r}_i,t)$ detected at each one of the pressure sensors, located at positions $\boldsymbol{r}_i$. The estimated acoustic strength $\tilde{q}(\boldsymbol{r},t)$ is calculated by applying the relative delays to the acoustic signal of the $i$-th channel and averaging across the $N$ channels (Choi et al., 2014):

$$\tilde{q}(\boldsymbol{r},t)=\frac{1}{N}\sum_{i=1}^{N}4\pi|\boldsymbol{r}_i-\boldsymbol{r}|\,w_i\,\tilde{p}\left(\boldsymbol{r}_i,t+|\boldsymbol{r}_i-\boldsymbol{r}|/c\right) \tag{2}$$

where $w_i$ is a weight applied to the $i$-th channel and is assumed to be equal to 1 in the previous approaches (Gyöngy and Coussios, 2010a; Gyöngy and Coviello, 2011). The estimated acoustic energy radiated by this single acoustic event can be simply calculated as:

$$\tilde{E}(\boldsymbol{r})=\frac{1}{4\pi\rho_0 c}\int_0^T\tilde{q}^2(\boldsymbol{r},t)\,dt \tag{3}$$

where $\rho_0$ is the water density set to 1000 kg/m$^3$ and $T$ is the total duration of the signal.

Conventional PAM – also known as time exposure acoustics (TEA) – has lateral and elevational resolutions of 0.27 mm and 2.35 mm with our settings, respectively (Gyöngy and Coussios, 2010a). These values are the -3 dB resolutions of the passive acoustic maps and were calculated using the centre frequency and aperture size of the L7-4 imaging probe, which were 5.2 MHz and 32 mm respectively. The calculation was conducted at an imaging depth of 37 cm, which coincided with the elevational location of the tube. For comparison, the therapeutic transducer's lateral beamwidth was 5.85 mm. The poor axial resolution is

exacerbated by an artefact in the form of a "tail effect", which is the detection of acoustic activity towards and away from the array that does not correspond to real acoustic emissions (Choi and Coussios, 2012; Gyöngy and Coussios, 2010a, 2010b). This artefact has been attributed to diffraction patterns on the array (Haworth et al., 2012) and to signal interference from multiple bubbles scattering within the region of interest and has been reduced via robust Capon beamforming (Coviello et al., 2015).

The robust Capon beamforming algorithm (RCB) (Coviello et al., 2015; Li et al., 2003; Stoica et al., 2003) was implemented here to suppress the interference patterns arising in the TEA algorithm. In brief, the Capon beamformer determines the apodization weights $w_i$ appearing in Eq. (2) to minimize the output power while maintaining unity gain in the direction of the focus (Åsen et al., 2014; Capon, 1969). This process reduces signals from non-focal directions and, alongside with the lateral, improves the axial resolution of the resulting beamformed image (Taki et al., 2012). RCB is a modification of the Capon beamformer which allows the calculation of energy without determining individual weights for each channel and has been shown to reduce the interference artefact outside the focal area (Coviello et al., 2015). All the 2D acoustic energy maps presented in this work are 81 × 21 pixel maps generated with the PAM-RCB algorithm, with a pixel size of 0.25 mm × 1 mm on the lateral and elevational directions respectively. The RCB epsilon value was kept constant and equal to 0.01 for all the processed data. Using this value, we generated maps with the least apparent activity outside the focal volume out of the values tested. To account for the global suppression of acoustic signals by the RCB algorithm, we rescaled the RCB map magnitudes based on TEA measurements.

***2. Symmetry estimation***

Our primary aim was to characterize the spatiotemporal distribution of acoustic cavitation activity within the focal volume. We have thus defined a symmetry index in order to assess the uniformity of the flowing microbubble activity in space and time. The focal area was separated into 2 different lateral (upstream and downstream) regions (Fig. 1(c)), since our setup was designed to produce elevationally symmetrical dynamics. We calculated the lateral uniformity index ($LU$) using the energy values measured within the tube in these regions. The symmetry index was calculated as follows:

$$LU = \frac{\tilde{E}_{downstream} - \tilde{E}_{upstream}}{\tilde{E}_{downstream} + \tilde{E}_{upstream}} \tag{4}$$

where $\tilde{E}$ denotes the energy measured in each compartment. Energy values were calculated by integrating the acoustic emissions over the entire acquisition length for a single PAM frame, i.e. for 150 μs. Based on our definition, $LU$ could obtain values between -1 and 1 in each frame, with -1 denoting 100% of the energy located upstream, and 1 denoting 100% of the energy located downstream. A value of 0 indicates symmetrical distribution. We compared the effect of the different pulse shapes and sequences on the basis of this spatiotemporal distribution metric.

***3. Acoustic cavitation analysis***

Although the magnitude of acoustic cavitation activity within a specified location is of great interest, it lacks information about the cavitation type. To elucidate these features from the acoustic energy emissions, we extracted the source strength time trace at three different points within the focal area (upstream, center and downstream points, shown as small green circles in Fig. 1(c)) and spectrally analysed the time-domain acoustic signal for every subsequent frame. For each imaging frame we performed Fast Fourier transforms (FFT) of the beamformed RF lines corresponding to the pixels of interest. FFTs were performed on the

entire 150μs time-domain trace of each distinct pulse for each pixel and were then gathered in spectrograms for the different parametric sets**.** We assessed the temporally-resolved spectral information in order to determine the cavitation mode in each spatial location over time, and identified potential inertial cavitation and/or collapse of the cavitation nuclei.

### C. High-speed video microscopy

To qualitatively confirm that the microbubbles are able to flow across the focal area during RaSP sonication, we conducted high-frame rate microscopy in a similar flow system (Fig. 1(a)). A round borosilicate glass capillary (inner diameter: 0.6mm, outer diameter: 0.84mm; length: 100mm; CM scientific, West Yorkshire, UK) was submerged into a water tank containing deionized water. Microbubble solution was continuously mixed using a magnetic stirrer and withdrawn at a steady fluid velocity of 10 mm/s. Our optical setup consisted of a 40x water-immersion objective (working distance: 3.3 mm, N.A.: 0.8, F.N.: 26.5, part number: N2667700; Olympus Industrial, Essex, UK) mounted onto a bright-field microscope (Olympus Industrial, Essex, UK). A high-speed camera (Fastcam SA5; Photron Europe Ltd., West Wycombe, UK) was attached to the microscope and enabled capturing of high-speed videos. We recorded videos with a field-of-view of $250\times237\,\mu m^2$ (893×846 pixels) at 10 kfps. We selected such a field-of-view in order to depict as many microbubbles as possible. Optical observations were used to confirm our hypothesis of short-pulse sequences allowing microbubble cloud mobility during the off-time. No further quantification of the individual microbubble dynamics was performed.

## III. RESULTS AND DISCUSSION

### A. Passive Acoustic Mapping

#### *1. Temporal evolution of cavitation energy*

The total acoustic output generated by sonication with a RaSP sequence was expected to be lower than with a 100-ms-long pulse. This was confirmed by the measurement of acoustic emissions from the focal area, where the short pulses produced lower energy than long pulses during the first few milliseconds of sonication. For example, at a peak-rarefactional pressure (PRP) of 146 kPa the measured acoustic energy generated by the first pulse was lower by 81 ± 62 %, 37 ± 33 %, and 36 ± 31 % for PLs of 5, 25, and 50 cycles, respectively, when compared to the long pulse (Fig. 3). Despite the lower total energy produced at a PL of 5 cycles, it was far more consistent throughout the sonication duration (Fig. 3(a)). In contrast, the long pulse had a very high initial energy output, but this diminished rapidly over time. Lower pulse lengths sustained cavitation activity for a longer duration, with the PL of 5 cycles generating emissions for the entire sonication duration in most of the tested RaSP sequences.

***2. Spatiotemporal distribution of cavitation activity***

We hypothesized that enhanced cavitation persistence in a flow environment could improve the distribution of cavitation activity within the focus, because it would allow microbubbles to move with the flow during the pulse repetition intervals. Passive acoustic maps confirmed this hypothesis, showing that RaSP sequences produced less biased distributions of microbubble-seeded acoustic activity than long pulses.

At low pressures (PRP: 298 kPa), the first pulse generally produced a uniform distribution within the focal volume (Fig. 4, top). During long-PL exposures the energy of acoustic emissions diminished rapidly and was 5x lower by 25 ms (with respect to the first acquired frame) and resulted in a less uniform distribution (Fig. 4, center). In contrast, the energy after 25 ms of 5-cycle RaSP sonication decreased by only 1.7x. By 50ms, the distribution remained uniform for the PL of 5 cycles, but was progressively less uniform for

longer PLs (Fig. 4, bottom). Furthermore, the maximum energy measured within the focus decreased by 80x for the long pulse, and 2.4x for the 5-cycle RaSP sonication.

Similar trends were observed across the different acoustic pressures evaluated although at different rates (data not shown). Loss of uniformity occurred faster at higher acoustic pressures due to the faster destruction of the cavitation nuclei. Interestingly, even for pressures well above the inertial cavitation threshold (e.g. PRP of 900 kPa), 5-cycle sonication instigated a spatiotemporally uniform distribution of acoustic activity.

Cumulative maps of acoustic energy over the entire sonication duration were assessed to evaluate the overall distribution of cavitation. An example of a map generated by high pressure sonication is given in figure 5 (PRP: 603 kPa). For the long pulse control, we observed an upstream spatial bias in the magnitude of the acoustic emissions (Fig. 5, far right) that was in accordance with previous studies (Choi and Coussios, 2012). Sonication with the RaSP sequences generated a more uniform distribution of acoustic cavitation emissions throughout the focal volume (Fig. 5, far left). Shorter pulses generated a better distribution than longer (Fig. 5 inner left and inner right). In agreement with the aforementioned focal energy measurements (Fig. 3), the emitted source energies in the cumulative maps increased with the pulse length (Fig. 5). Thus, we observed a trade-off between the uniformity and magnitude of acoustic cavitation activity.

### *3. Cavitation type*

In order to understand the cause of the observed biases in cavitation distribution, we spectrally analyzed the acoustic emissions to determine the type of cavitation generated (PRP: 298 kPa, Fig. 6). Sonication at 298 kPa produced dynamics that are representative of different pressures and was further analyzed here. The most immediate observation was that broadband emissions were observed for all pulse lengths at this pressure. This indicates that

high magnitude inertial cavitation was present and caused transient events and possibly microbubble fragmentation. Broadband emissions were stronger and persisted longer at the upstream and central pixel locations of the focal volume, which indicate that microbubbles flowing into the focal volume were being destroyed (Fig. 6, top and center).

The magnitude and the duration of the broadband signal varied with pulse length. By increasing the pulse length, the magnitude of the broadband emissions increased while their duration generally decreased (Fig. 6, top and bottom). These observations are compatible with previous studies that investigated the likelihood of transient inertial cavitation as a function of acoustic pressure (Apfel and Holland, 1991; Gruber et al., 2014). Strong harmonic and broadband emissions were generally observed at the upstream point of the focus (Fig. 6, top), due to the replenishment of the focal volume with fresh cavitation nuclei. Broadband emissions were detected also at the lowest pressure tested (PRP: 146 kPa), although at a lower magnitude (data not shown).

Flowing microbubbles that enter the focus were destroyed or modified by the acoustic field and produced a recurring mixture of cavitation dynamics in the upstream portion of the beam. Meanwhile, harmonic or broadband emissions downstream to the flow were not as strong (Fig. 6, bottom). The short length of the 5-cycle pulse caused spectral broadening, which made discrimination of the harmonic emissions from the broadband events difficult. However, the trends of the broadband emissions observed in the larger PLs appeared also in the 5-cycle spectrograms. In general, spectral analysis showed that the rate of microbubble destruction increased with the pulse length.

### *4. Lateral distribution of cavitation activity*

We characterized the lateral distribution of acoustic source power through the focal point to understand how cavitation activity evolved over time for different pulse sequences

(Fig. 7). As shown in figure 3, short-pulse sonication (PL: 5 cycles) maintained a uniform acoustic cavitation activity for a longer duration compared to longer PLs and the long-pulse control (Fig. 7, top). At PRPs higher than 300kPa, cavitation activity was substantial only during the first 1 to 3 ms of sonication, followed by a rapid decrease (Fig. 7, right). In contrast, RaSP sequences maintained similar levels of acoustic activity for up to 10ms of sonication (for the PL of 5 cycles). Microbubbles sonicated with a PRP of 298kPa with PLs of 5, 25, 50, and 50,000 cycles were active for up to 65, 125, 100 and 500 cycles, respectively. Our data suggests that microbubbles do not last longer per unit of ultrasound on-time in RaSP sonication. Interestingly, prolonged cavitation activity using RaSP sequences was observed even at a PRP of 900 kPa, which is well above the inertial cavitation threshold (Fig. 7, left). This is in accordance with previous studies that showed a correlation between the pulse length and the inertial cavitation dose (Chen et al., 2003a, 2003b). Taken together, these data suggest that the enhanced microbubble lifetime in RaSP sonication is caused by a combined effect of short pulse length and increased inertial cavitation threshold.

***5. Symmetry index to assess spatiotemporal uniformity***

To quantify our observations, we calculated the mean lateral uniformity along the tube length using Eq. (4). Averaging was conducted across three repetitions for each experimental parameter (Fig. 8). The lateral uniformity index for the long-pulse control generally had initial values close to 0 but progressively shifted towards negative values (i.e. upstream bias). $LU$ was consistently negative for long-pulse sonication due to the destruction of the incoming nuclei (Fig. 8, right). In contrast, 5-cycle sonication consistently produced laterally uniform distribution (i.e., $LU \approx 0$), especially at a PRP of 146 kPa (Fig. 8, left). Although higher pressures yielded higher variability across the samples, generally the lateral uniformity index was close to 0 for 5-cycle sonication, demonstrating an improvement to the acoustic

activity lateral distribution. Large standard deviations were measured in the *LU* of long-pulse sonication across the acoustic pressures. This reflects the unpredictability and variability of acoustic cavitation distribution with each pulse. Generally, short pulses produced less variation in the *LU* values, demonstrating a more consistent and uniform distribution of cavitation activity.

**B. High-speed video microscopy**

We performed high-speed microscopy observations in a setup similar to the PAM experiment to optically observe individual microbubble movement. Our observations showed that the translational dynamics of the microbubbles at low acoustic pressures were primarily affected by secondary radiation forces during the on-time of the pulse sequence (Dayton et al., 2002). At longer PLs, secondary forces were exerted in the vicinity of each bubble over a longer time period, resulting in fast cluster formation (Fig. 9(b)), as expected (Chen et al., 2016; Fan et al., 2014). Microbubble clusters moved away from the transducer as a whole under the influence of primary radiation forces. In contrast, at low-duty-cycle sonication, microbubbles were attracted to each other during the short on-time, but moved freely due to the fluid drag force during the off-time of the sequence (Fig. 9(a), see supplementary video). Hence, our hypothesis of enhanced mobility of the flowing cavitation nuclei during the entire sonication period was confirmed. At higher pressures microbubbles within the focus were either immediately destroyed or disappeared from the field-of-view due to primary radiation forces.

**C. Clinical importance.**

RaSP sequences have been recently shown to enhance drug delivery rates in blood-barrier opening studies (Choi et al., 2011a, 2011b). Pulses as short as 2.3 μs emitted at PRFs on the order of kHz were shown to produce the desired bioeffect, i.e. noninvasively enhance

vascular permeability within the brain without neuronal damage or erythrocyte extravasation (Choi et al., 2011b). In contrast, long-pulse sonication resulted in accumulation of the model drug near large vessels and in a heterogeneous drug distribution within the targeted hippocampi of the mouse brains (Choi et al., 2007b, 2010, 2011a). The physical basis of this difference, as proposed previously (Pouliopoulos et al., 2014) and confirmed here, is the distribution of acoustic cavitation activity within a treatment volume. We have demonstrated that the upstream bias produced by long-pulse sonication (Choi and Coussios, 2012) can be greatly reduced by RaSP sonication (Fig. 4,5,7, and 8). This improved distribution may allow for more favourable cavitation dynamics where they are needed and reduce the overtreatment of regions.

RaSP sonication can be implemented in a variety of *in vivo* applications such as blood-brain barrier opening (Hynynen et al., 2001; Konofagou, 2012), sonoporation (Hu et al., 2013; Shamout et al., 2015; Zhou et al., 2008), clot dissolution (Bader et al., 2015; Holland et al., 2002) and targeted drug delivery (Ferrara et al., 2007). Cancer treatment is expected to benefit from RaSP sequence sonication, since a uniform drug distribution within the tumour core and periphery is essential for successful treatment. Focused ultrasound in conjunction with circulating microbubbles have been used to enhance the intratumoral concentration of liposomes, adenoviruses, genes and antibodies (Carlisle et al., 2013; Choi et al., 2014; Graham et al., 2014; Liao et al., 2015; Nomikou and McHale, 2012). Inertial cavitation followed by microbubble collapse was proved to increase the delivered doses even at large distances away from the vessel lumen. In spite of this significant increase, the lack of control of cavitation dynamics in the focus resulted in a inhomogeneous drug distribution within the tumour (Graham et al., 2014; Liao et al., 2015). PAM data have suggested that there is a higher magnitude of acoustic cavitation activity at the distal to the skin part of the targeted tumour, on the edge of the targeted area (Choi et al., 2014). We speculate that this result

stems from the destruction of microbubbles flowing into the acoustic focus through the tortuous tumour vasculature (Kim et al., 2012), yielding an upstream bias as shown in our *in vitro* setup (Fig. 4, 5 and 6). It has been also reported that the drug delivery distribution is correlated with the acoustic cavitation distribution, and that the latter can be assessed in real-time using RCB-PAM (Choi et al., 2014).

Although we were able to distribute the cavitation activity throughout the focal volume, the produced emissions magnitude was lower than the conventional therapy (Fig. 3 and 5). This was expected due to the lower acoustic input, yet it may affect the outcome of therapeutic applications, since most studies employ inertial cavitation to trigger the desired bioeffect (Choi et al., 2014; Graham et al., 2014). High magnitude inertial cavitation produces higher stress within the vasculature (Hosseinkhah et al., 2013), but is associated with non-uniform effects and strong upstream bias (Fig. 4,5,6). Thus, our target is to achieve the right magnitude of acoustic cavitation activity at the right location. Higher magnitudes can be achieved by increasing the acoustic pressure of RaSP sonication, thus increasing the acoustic energy input. To evaluate the *in vivo* potential of the described rapid short-pulse sequences, we aim to apply this method to achieve targeted drug delivery for the treatment of breast cancer and Alzheimer's disease.

The uniformity index defined in the present work (Eq. 4) can be used in feedback-loop systems based on RCB-PAM, for the real-time monitoring and adjustment of the emitted pulse shape and sequence. Future targeted drug delivery systems could calculate symmetry metrics in real-time, and modify the emitted acoustic pressure, pulse length, and pulse repetition frequency in order to minimize the lateral uniformity index (Fig. 8) while maintaining a high magnitude of acoustic emissions over time (Fig. 3(a)). In a non-symmetrical environment, the lateral uniformity index can be complemented with an

elevational uniformity index, to take into account the full 2D spatiotemporal distribution of acoustic cavitation activity.

**D. Limitations of the study.**

Our simple setup modelled the flow of a microbubble cloud within the vasculature. Although this setup offered insight on the spatiotemporal dynamics of cavitation activity within the focal volume, it does not fully capture the diversity and complexity of *in vivo* vascular networks. Similar uniformity trends are expected in an *in vivo* vascular network, assuming continuous flow of cavitation nuclei through, for example, a capillary bed. This assumption may be valid in healthy arteries, veins or microvessels, but it does not apply to irregular vasculature. For instance, blood flow is considerably heterogeneous in the tumour vasculature (Kim et al., 2012; Zhu et al., 2013), thus a different cavitation distribution is expected within the tumour microenvironment.

Individual microbubbles change their dynamic behaviour when oscillating next to a boundary such as the capillary wall (Chen et al., 2012; Garbin et al., 2007; Martynov et al., 2009). Microbubble dynamics are also likely to be affected *in vivo* by the presence of other molecules and cells within the blood. Inertial cavitation has been show to occur at higher pressures in blood than in saline (Apfel and Holland, 1991). Hence a different acoustic response is expected *in vivo*. An additional disadvantage of a large tube as opposed to a vascular bed is the close vicinity of the individual cavitation nuclei which affects the magnitude of their interaction and hence the collective oscillation modes of the microbubble cloud (Zeravcic et al., 2011). Furthermore, the vascular network is surrounded by a complex musculoskeletal environment that can cause reflections or aberrations of the acoustic beam. These distortions could result in different acoustic cavitation distributions than those presented in this work, where water was used as surrounding material.

## IV. CONCLUSIONS

We have shown here that RaSP ultrasound exposure is able to reduce or eliminate the non-uniform effects and the upstream spatial bias produced by long-pulse exposure. Sonication with short pulses separated with μs off-times was shown to sustain uniform acoustic emissions and to reduce the effect primary and secondary radiation forces over time. By extending the microbubble lifetime and enhancing their mobility, we were able to spread the acoustic activity in space and time. We observed a trade-off between the spatiotemporal uniformity and the total energy of cavitation activity within the focal volume using RaSP sonication. RCB-PAM provided spatially-resolved acoustic cavitation activity in real-time, hence constituting a powerful tool for the monitoring and adjustment of the ultrasound emission characteristics. Rapid short-pulse sequences and RCB-PAM in conjunction with the symmetry index can be thus used to increase the control of acoustic cavitation dynamics in future *in vivo* applications.

## ACKNOWLEDGEMENTS

The authors would like to thank Mr. Sinan Li and Mr. Chee Hau Leow for their assistance with the Verasonics research platform and Mr. Gary Jones for building the experimental apparatuses. M.T. acknowledges the support of the Swiss National Science Foundation (grant P2ELP2_151953). This work was funded by the Wellcome Trust Institutional Strategic Support Fund to Imperial College London.

## REFERENCES


Apfel, R. (**1997**). "Sonic effervescence: A tutorial on acoustic cavitation," J. Acoust. Soc. Am., **101**, 1227–1237.

Apfel, R. E., and Holland, C. K. (**1991**). "Gauging the likelihood of cavitation from short-pulse, low-duty cycle diagnostic ultrasound," Ultrasound Med. Biol., **17**, 179–85.

Åsen, J. P., Buskenes, J. I., Colombo Nilsen, C.-I., Austeng, A., and Holm, S. (**2014**). "Implementing capon beamforming on a GPU for real-time cardiac ultrasound imaging," IEEE Trans. Ultrason. Ferroelectr. Freq. Control, **61**, 76–85. doi:10.1109/TUFFC.2014.6689777

Bader, K. B., Gruber, M. J., and Holland, C. K. (**2015**). "Shaken and stirred: mechanisms of ultrasound-enhanced thrombolysis," Ultrasound Med. Biol., **41**, 187–96. doi:10.1016/j.ultrasmedbio.2014.08.018

Baseri, B., Choi, J. J., Tung, Y.-S., and Konofagou, E. E. (**2010**). "Multi-modality safety assessment of blood-brain barrier opening using focused ultrasound and definity microbubbles: a short-term study," Ultrasound Med. Biol., **36**, 1445–59. doi:10.1016/j.ultrasmedbio.2010.06.005

Borden, M. A., and Longo, M. L. (**2002**). "Dissolution Behavior of Lipid Monolayer-Coated, Air-Filled Microbubbles: Effect of Lipid Hydrophobic Chain Length," Langmuir, **18**, 9225–9233. doi:10.1021/la026082h

Capon, J. (**1969**). "High-resolution frequency-wavenumber spectrum analysis," Proc. IEEE,. doi:10.1109/PROC.1969.7278

Carlisle, R., Choi, J., Bazan-Peregrino, M., Laga, R., Subr, V., Kostka, L., Ulbrich, K., Coussios, C.C., and Seymour, L.W. (**2013**). "Enhanced tumor uptake and penetration of virotherapy using polymer stealthing and focused ultrasound," J. Natl. Cancer Inst., **105**, 1701–1710. doi:10.1093/jnci/djt305

Chen, H., Brayman, A., and Matula, T. J. (**2012**). "Characteristic microvessel relaxation timescales associated with ultrasound-activated microbubbles," Appl. Phys. Lett., **101**, 163704. doi:10.1063/1.4761937

Chen, W. S., Brayman, A. A., Matula, T. J., Crum, L. A., and Miller, M. W. (**2003**). "The pulse length-dependence of inertial cavitation dose and hemolysis," Ultrasound Med. Biol., **29**, 739–748. doi:10.1016/S0301-5629(03)00029-2

Chen, W.-S., Brayman, A. A., Matula, T. J., and Crum, L. A. (**2003**). "Inertial cavitation dose and hemolysis produced in vitro with or without Optison," Ultrasound Med. Biol., **29**, 725–37.

Chen, X., Wang, J., Pacella, J. J., and Villanueva, F. S. (**2016**). "Dynamic Behavior of Microbubbles during Long Ultrasound Tone-Burst Excitation: Mechanistic Insights into Ultrasound-Microbubble Mediated Therapeutics Using High-Speed Imaging and Cavitation Detection," Ultrasound Med. Biol., **42**, 528–38. doi:10.1016/j.ultrasmedbio.2015.09.017

Choi, J. J., Carlisle, R. C., Coviello, C., Seymour, L., and Coussios, C.-C. (**2014**). "Non-invasive and real-time passive acoustic mapping of ultrasound-mediated drug delivery," Phys. Med. Biol., **59**, 4861–4877. doi:10.1088/0031-9155/59/17/4861

Choi, J. J., and Coussios, C.-C. (**2012**). "Spatiotemporal evolution of cavitation dynamics exhibited by flowing microbubbles during ultrasound exposure," J. Acoust. Soc. Am., **132**, 3538–49. doi:10.1121/1.4756926

Choi, J. J., Pernot, M., Small, S. A., and Konofagou, E. E. (**2007**). "Noninvasive, transcranial and localized opening of the blood-brain barrier using focused ultrasound in mice," Ultrasound Med. Biol., **33**, 95–104. doi:10.1016/j.ultrasmedbio.2006.07.018

Choi, J. J., Selert, K., Gao, Z., Samiotaki, G., Baseri, B., and Konofagou, E. E. (**2011**). "Noninvasive and localized blood-brain barrier disruption using focused ultrasound can be achieved at short pulse lengths and low pulse repetition frequencies," J. Cereb. Blood Flow Metab., **31**, 725–37. doi:10.1038/jcbfm.2010.155

Choi, J. J., Selert, K., Vlachos, F., Wong, A., and Konofagou, E. E. (**2011**). "Noninvasive and localized neuronal delivery using short ultrasonic pulses and microbubbles," Proc. Natl. Acad. Sci. U. S. A., **108**, 16539–44. doi:10.1073/pnas.1105116108

Choi, J. J., Wang, S., Tung, Y.-S., Morrison, B., and Konofagou, E. E. (**2010**). "Molecules of various pharmacologically-relevant sizes can cross the ultrasound-induced blood-brain barrier opening in vivo," Ultrasound Med. Biol., **36**, 58–67. doi:10.1016/j.ultrasmedbio.2009.08.006

Choi, J., Pernot, M., Brown, T. R., Small, S., and Konofagou, E. E. (**2007**). "Spatio-temporal analysis of molecular delivery through the blood-brain barrier using focused ultrasound," Phys. Med. Biol., **52**, 5509–30. doi:10.1088/0031-9155/52/18/004

Chomas, J. E., Dayton, P., May, D., and Ferrara, K. (**2001**). "Threshold of fragmentation for ultrasonic contrast agents," J. Biomed. Opt., **6**, 141–50. doi:10.1117/1.1352752

Church, C., and Carstensen, E. (**2001**). "'Stable' inertial cavitation," Ultrasound Med. Biol., **27**, 1435–1437.

Cosgrove, D. (**2006**). "Ultrasound contrast agents: an overview," Eur. J. Radiol., **60**, 324–30. doi:10.1016/j.ejrad.2006.06.022

Coussios, C. C., and Roy, R. A. (**2008**). "Applications of Acoustics and Cavitation to Noninvasive Therapy and Drug Delivery," Annu. Rev. Fluid Mech., **40**, 395–420. doi:10.1146/annurev.fluid.40.111406.102116

Coviello, C., Kozick, R., Choi, J., Gyöngy, M., Jensen, C., Smith, P. P., and Coussios, C.-C. (**2015**). "Passive acoustic mapping utilizing optimal beamforming in ultrasound therapy monitoring," J. Acoust. Soc. Am., **137**, 2573. doi:10.1121/1.4916694

Dalecki, D. (**2004**). "Mechanical bioeffects of ultrasound," Annu. Rev. Biomed. Eng., **6**, 229–48. doi:10.1146/annurev.bioeng.6.040803.140126

Dayton, P. A., Allen, J. S., and Ferrara, K. W. (**2002**). "The magnitude of radiation force on ultrasound contrast agents," J. Acoust. Soc. Am., **112**, 2183. doi:10.1121/1.1509428

Deelman, L. E., Declèves, A.-E., Rychak, J. J., and Sharma, K. (**2010**). "Targeted renal therapies through microbubbles and ultrasound," Adv. Drug Deliv. Rev., **62**, 1369–77. doi:10.1016/j.addr.2010.10.002

Fan, Z., Chen, D., and Deng, C. X. (**2014**). "Characterization of the dynamic activities of a population of microbubbles driven by pulsed ultrasound exposure in sonoporation," Ultrasound Med. Biol., **40**, 1260–72. doi:10.1016/j.ultrasmedbio.2013.12.002

Ferrara, K., Pollard, R., and Borden, M. (**2007**). "Ultrasound microbubble contrast agents: fundamentals and application to gene and drug delivery," Annu. Rev. Biomed. Eng., **9**, 415–447. doi:10.1146/annurev.bioeng.8.061505.095852

Fischer, K., McDannold, N. N. J., Zhang, Y., Kardos, M., Szabo, A. A., Reusz, G. S., and Jolesz, F. A. (**2009**). "Renal ultrafiltration changes induced by focused US," Radiology, **253**, 697–705. doi:10.1148/radiol.2532082100

Flynn, H. G. (**1982**). "Generation of transient cavities in liquids by microsecond pulses of ultrasound," J. Acoust. Soc. Am., **72**, 1926. doi:10.1121/1.388622

Garbin, V., Cojoc, D., Ferrari, E., Di Fabrizio, E., Overvelde, M. L. J., van der Meer, S. M., de Jong, N., et al. (**2007**). "Changes in microbubble dynamics near a boundary revealed by combined optical micromanipulation and high-speed imaging," Appl. Phys. Lett., **90**, 114103. doi:10.1063/1.2713164

Goertz, D. E., Wright, C., and Hynynen, K. (**2010**). "Contrast agent kinetics in the rabbit brain during exposure to therapeutic ultrasound," Ultrasound Med. Biol., **36**, 916–24. doi:10.1016/j.ultrasmedbio.2010.03.005

Graham, S. M., Carlisle, R., Choi, J. J., Stevenson, M., Shah, A. R., Myers, R. S., Fisher, K., Pelegrino, M. B., Seymour, L., and Coussios, C.-C. (**2014**). "Inertial cavitation to non-invasively trigger and monitor intratumoral release of drug from intravenously delivered liposomes," J. Control. release, **178**, 101–7. doi:10.1016/j.jconrel.2013.12.016

Gruber, M. J., Bader, K. B., and Holland, C. K. (**2014**). "Cavitation thresholds of contrast agents in an in vitro human clot model exposed to 120-kHz ultrasound," J. Acoust. Soc. Am., **135**, 646–653. doi:10.1121/1.4843175

Gyongy, M., Arora, M., Noble, J. A., and Coussios, C. C. (**2008**). "Use of passive arrays for characterization and mapping of cavitation activity during HIFU exposure," 2008 IEEE Ultrason. Symp., IEEE, 871–874. doi:10.1109/ULTSYM.2008.0210

Gyöngy, M., and Coussios, C.-C. (**2010**). "Passive cavitation mapping for localization and tracking of bubble dynamics," J. Acoust. Soc. Am., **128**, EL175–80. doi:10.1121/1.3467491

Gyöngy, M., and Coussios, C.-C. (**2010**). "Passive spatial mapping of inertial cavitation during HIFU exposure," IEEE Trans. Biomed. Eng., **57**, 48–56. doi:10.1109/TBME.2009.2026907

Gyöngy, M., and Coviello, C. M. (**2011**). "Passive cavitation mapping with temporal sparsity constraint," J. Acoust. Soc. Am., **130**, 3489–97. doi:10.1121/1.3626138

Haworth, K. J., Mast, T. D., Radhakrishnan, K., Burgess, M. T., Kopechek, J. a., Huang, S.-L., McPherson, D. D., and Holland, C.K. (**2012**). "Passive imaging with pulsed ultrasound insonations," J. Acoust. Soc. Am., **132**, 544. doi:10.1121/1.4728230

Helfield, B. L., and Goertz, D. E. (**2013**). "Nonlinear resonance behavior and linear shell estimates for Definity™ and MicroMarker™ assessed with acoustic microbubble spectroscopy," J. Acoust. Soc. Am., **133**, 1158–68. doi:10.1121/1.4774379

Hockham, N., Coussios, C. C., and Arora, M. (**2010**). "A real-time controller for sustaining thermally relevant acoustic cavitation during ultrasound therapy," IEEE Trans. Ultrason. Ferroelectr. Freq. Control, **57**, 2685–94. doi:10.1109/TUFFC.2010.1742

Holland, C. K., Vaidya, S. S., Coussios, C.-C., and Shaw, G. J. (**2002**). "Thrombolytic effects

of 120-kHz and 1-MHz ultrasound and tissue plasminogen activator on porcine whole blood clots," J. Acoust. Soc. Am., **112**, 2370. doi:10.1121/1.4779616

Hosseinkhah, N., Chen, H., Matula, T. J., Burns, P. N., and Hynynen, K. (**2013**). "Mechanisms of microbubble-vessel interactions and induced stresses: a numerical study," J. Acoust. Soc. Am., **134**, 1875–85. doi:10.1121/1.4817843

Hu, Y., Wan, J. M. F., and Yu, A. C. H. (**2013**). "Membrane perforation and recovery dynamics in microbubble-mediated sonoporation," Ultrasound Med. Biol., **39**, 2393–405. doi:10.1016/j.ultrasmedbio.2013.08.003

Hynynen, K., McDannold, N., Vykhodtseva, N., and Jolesz, F. A. (**2001**). "Noninvasive MR imaging-guided focal opening of the blood-brain barrier in rabbits," Radiology, **220**, 640–646. doi:10.1148/radiol.2202001804

Kim, E., Stamatelos, S., Cebulla, J., Bhujwalla, Z. M., Popel, A. S., and Pathak, A. P. (**2012**). "Multiscale imaging and computational modeling of blood flow in the tumor vasculature," Ann. Biomed. Eng., **40**, 2425–41. doi:10.1007/s10439-012-0585-5

Konofagou, E. E. (**2012**). "Optimization of the ultrasound-induced blood-brain barrier opening," Theranostics, **2**, 1223–37. doi:10.7150/thno.5576

Koruk, H., El Ghamrawy, A., Pouliopoulos, A. N., and Choi, J. J. (**2015**). "Acoustic Particle Palpation for Measuring Tissue Elasticity," Appl. Phys. Lett., **107**, 223701–04. doi:http://dx.doi.org/10.1063/1.4936345

Li, J., Stoica, P., and Wang, Z. (**2003**). "On robust Capon beamforming and diagonal loading," Signal Process. IEEE Trans.,. doi:10.1109/TSP.2003.812831

Liao, A. H., Chou, H. Y., Hsieh, Y. L., Hsu, S. C., Wei, K. C., and Liu, H. L. (**2015**). "Enhanced therapeutic epidermal growth factor receptor (EGFR) antibody delivery via pulsed ultrasound with targeting microbubbles for glioma treatment," J. Med. Biol. Eng., **35**, 156–164. doi:10.1007/s40846-015-0032-9

Lindner, J. R. (**2004**). "Microbubbles in medical imaging: current applications and future directions," Nat. Rev. Drug Discov., **3**, 527–32. doi:10.1038/nrd1417

Liu, H.-L., Wai, Y.-Y., Chen, W.-S., Chen, J.-C., Hsu, P.-H., Wu, X.-Y., Huang, W.-C., Yen, T.-C., and Wang, J.-J. (**2008**). "Hemorrhage detection during focused-ultrasound induced blood-brain-barrier opening by using susceptibility-weighted magnetic resonance imaging," Ultrasound Med. Biol., **34**, 598–606. doi:10.1016/j.ultrasmedbio.2008.01.011

Marmottant, P., van der Meer, S., Emmer, M., Versluis, M., de Jong, N., Hilgenfeldt, S., and Lohse, D. (**2005**). "A model for large amplitude oscillations of coated bubbles accounting for buckling and rupture," J. Acoust. Soc. Am., **118**, 3499. doi:10.1121/1.2109427

Martynov, S., Stride, E., and Saffari, N. (**2009**). "The natural frequencies of microbubble oscillation in elastic vessels," J. Acoust. Soc. Am., , doi: 10.1121/1.3243292. doi:10.1121/1.3243292

van der Meer, S. M., Dollet, B., Voormolen, M. M., Chin, C. T., Bouakaz, A., de Jong, N., Versluis, M., and Lohse, D. (**2007**). "Microbubble spectroscopy of ultrasound contrast agents," J. Acoust. Soc. Am., **121**, 648. doi:10.1121/1.2390673

Nomikou, N., and McHale, A. P. (**2012**). "Microbubble-enhanced ultrasound-mediated gene

transfer--towards the development of targeted gene therapy for cancer," Int. J. Hyperthermia, **28**, 300–10. doi:10.3109/02656736.2012.659235

O'Reilly, M. A., and Hynynen, K. (**2012**). "Blood-Brain Barrier: Real-time Feedback-controlled Focused Ultrasound Disruption by Using an Acoustic Emissions–based Controller," Radiology, **263**, 96–106. doi:10.1148/radiol.11111417

O'Reilly, M. a., Waspe, A. C., Ganguly, M., and Hynynen, K. (**2011**). "Focused-Ultrasound Disruption of the Blood-Brain Barrier Using Closely-Timed Short Pulses: Influence of Sonication Parameters and Injection Rate," Ultrasound Med. Biol., **37**, 587–594. doi:10.1016/j.ultrasmedbio.2011.01.008

Palanchon, P., Tortoli, P., Versluis, M., and de Jong, N. (**2005**). "Optical observations of acoustical radiation force effects on individual air bubbles," IEEE Trans. Ultrason. Ferroelectr. Freq. Control, **52**, 104–110.

Pouliopoulos, A. N., Bonaccorsi, S., and Choi, J. J. (**2014**). "Exploiting flow to control the in vitro spatiotemporal distribution of microbubble-seeded acoustic cavitation activity in ultrasound therapy," Phys. Med. Biol., **59**, 6941–6957. doi:10.1088/0031-9155/59/22/6941

Salgaonkar, V. A., Datta, S., Holland, C. K., and Mast, T. D. (**2009**). "Passive cavitation imaging with ultrasound arrays," J. Acoust. Soc. Am., **126**, 3071–83. doi:10.1121/1.3238260

Shamout, F. E., Pouliopoulos, A. N., Lee, P., Bonaccorsi, S., Towhidi, L., Krams, R., and Choi, J. J. (**2015**). "Enhancement of Non-invasive Trans-membrane Drug Delivery Using Ultrasound and Microbubbles during Physiologically Relevant Flow," Ultrasound Med. Biol., **41**, 2435–2448. doi:10.1016/j.ultrasmedbio.2015.05.003

Stieger, S. M., Caskey, C. F., Adamson, R. H., Qin, S., Curry, F.-R. E., Wisner, E. R., and Ferrara, K. W. (**2007**). "Enhancement of Vascular Permeability with Low-Frequency Contrast-enhanced Ultrasound in the Chorioallantoic Membrane Model," Radiology, **243**, 112–121. doi:10.1148/radiol.2431060167

Stoica, P., Wang, Z., and Li, J. (**2003**). "Robust Capon beamforming," Signal Process. Lett. IEEE,. doi:10.1109/LSP.2003.811637

Stride, E. P., and Coussios, C. C. (**2010**). "Cavitation and contrast: the use of bubbles in ultrasound imaging and therapy," Proc. Inst. Mech. Eng. Part H J. Eng. Med., **224**, 171–191. doi:10.1243/09544119JEIM622

Stride, E., and Saffari, N. (**2003**). "Microbubble ultrasound contrast agents: A review," Proc. Inst. Mech. Eng. Part H J. Eng. Med. , **217** , 429–447. doi:10.1243/09544110360729072

Taki, H., Taki, K., Sakamoto, T., Yamakawa, M., Shiina, T., Kudo, M., and Sato, T. (**2012**). "High range resolution ultrasonographic vascular imaging using frequency domain interferometry with the Capon method," IEEE Trans. Med. Imaging, **31**, 417–29. doi:10.1109/TMI.2011.2170847

Tangelder, G. J., Slaaf, D. W., Muijtjens, a. M., Arts, T., oude Egbrink, M. G., and Reneman, R. S. (**1986**). "Velocity profiles of blood platelets and red blood cells flowing in arterioles of the rabbit mesentery," Circ. Res., **59**, 505–514. doi:10.1161/01.RES.59.5.505

Tung, Y.-S., Vlachos, F., Choi, J. J., Deffieux, T., Selert, K., and Konofagou, E. E. (**2010**).

"In vivo transcranial cavitation threshold detection during ultrasound-induced blood-brain barrier opening in mice," Phys. Med. Biol., **55**, 6141–55. doi:10.1088/0031-9155/55/20/007

Yu, H., and Xu, L. (**2014**). "Cell experimental studies on sonoporation: State of the art and remaining problems," J. Control. Release, **174**, 151–160. doi:10.1016/j.jconrel.2013.11.010

Zeravcic, Z., Lohse, D., and Van Saarloos, W. (**2011**). "Collective oscillations in bubble clouds," J. Fluid Mech., **680**, 114–149. doi:10.1017/jfm.2011.153

Zhou, Y., Cui, J., and Deng, C. X. (**2008**). "Dynamics of sonoporation correlated with acoustic cavitation activities," Biophys. J., **94**, L51–3. doi:10.1529/biophysj.107.125617

Zhu, Y., Li, F., Vadakkan, T. J., Zhang, M., Landua, J., Wei, W., Ma, J., Dickinson, M.A., Rosen, J.M., Lewis, M.T., Zhan, M., and Wong, S.T.C. (**2013**). "Three-dimensional vasculature reconstruction of tumour microenvironment via local clustering and classification," Interface Focus, **3**, 20130015. doi:10.1098/rsfs.2013.0015

## TABLES

Table I. Ultrasound and physiological parameters.

| | |
|---|---|
| Peak-rarefactional pressure (kPa) | 146, 298, 603, 900 |
| Pulse repetition frequency (kHz) | 1.25 |
| Pulse length (no. of cycles) | 5, 25, 50, 50,000 (control) |
| Flow rate (mm/s) | 10 |
| Burst length (ms) | 100 |

**FIGURES**

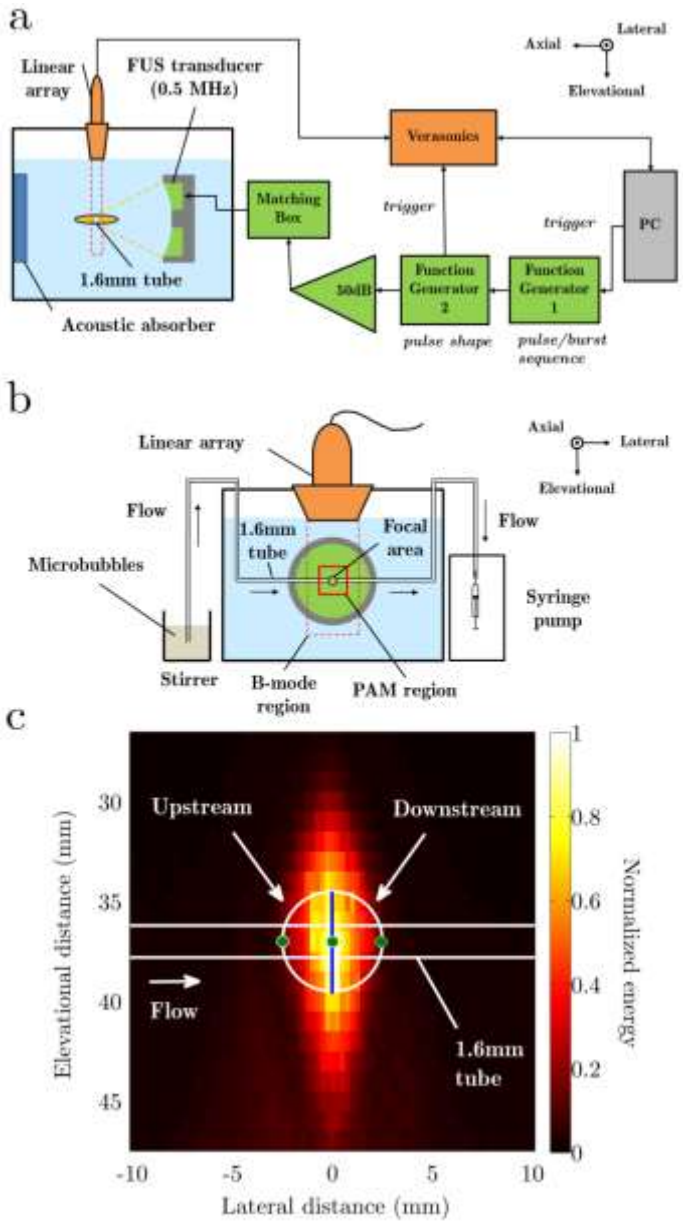


FIG. 1. (Color online) a) Experimental setup in side view (a) and front view (b). The rapid short-pulse sequences were generated with two function generators, one determining the pulse shape and the other the pulse sequence. A 0.5MHz focused ultrasound transducer was used to sonicate the flowing microbubbles while a linear array passively captured their acoustic emissions. Verasonics acquisition was triggered by function generator 2. c) Example of passive acoustic map separated to the symmetry metrics semicircles (upstream and

downstream, separated by the blue line) within the acoustic focus (white circle). Microbubbles are flowing from left (upstream) to right (downstream) in a tube with inner diameter of 0.8 mm and outer diameter of 1.6mm (white lines). Green circles denote the points at which spectral analysis was conducted.

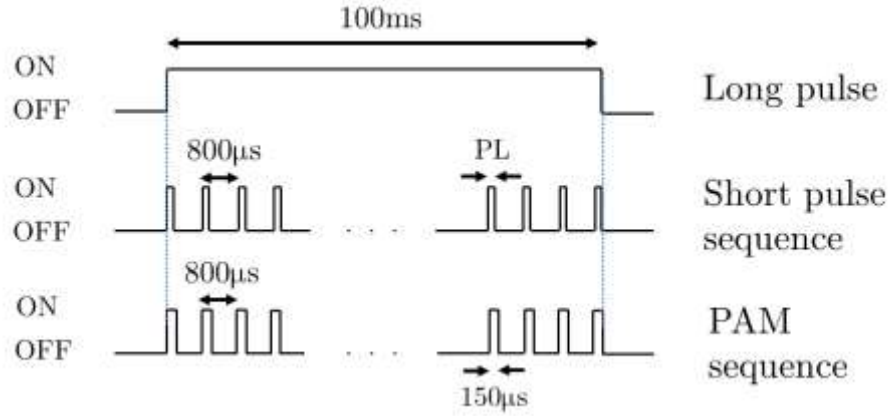


FIG. 2. Rapid short pulse sequences (center) compared with the long pulse gold standard (top) and the passive acoustic mapping (PAM) acquisition sequence (bottom). Emission and reception of acoustic signals were synchronised. Short-pulse microbubble signals fitted within the acquisition duration (center-bottom).

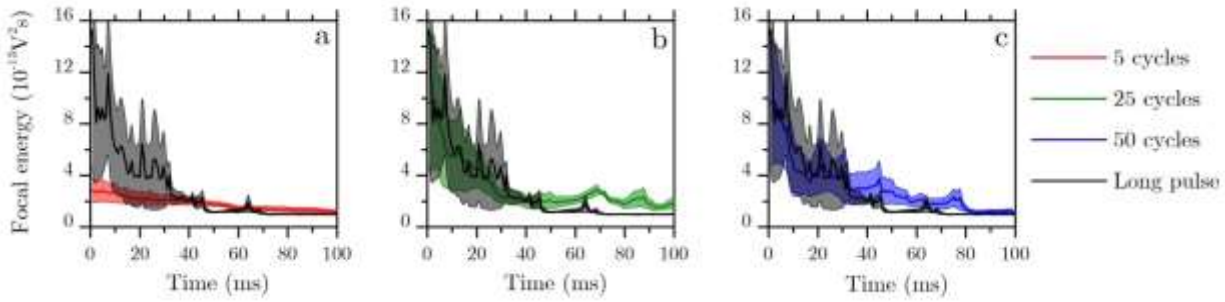


FIG. 3. (Color online) Temporal evolution of the mean focal energy. Comparison between the long-pulse control and (a) 5 cycles, (b) 25 cycles, and (c) 50 cycles. Short pulses yielded lower yet more stable acoustic emissions over time than the long pulse. PRP=146kPa, n=3 repetitions.

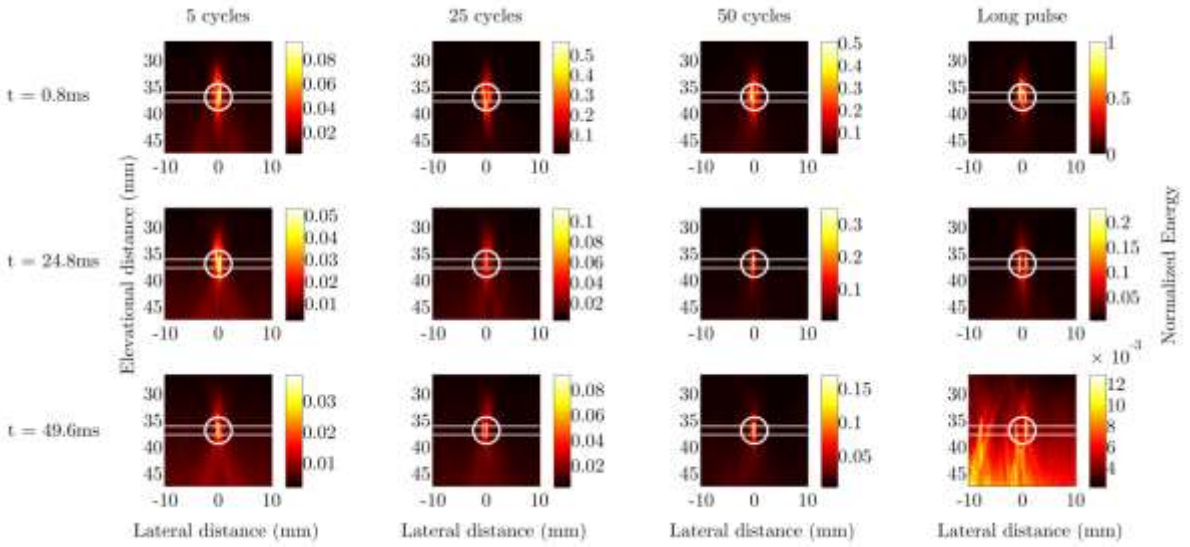


FIG. 4. (Color online) Passive acoustic maps for different pulse sequences at different time points (from top to bottom, t = 0.8, 24.8, 49.6 ms). All values are normalised to the first frame maximum energy at long pulse sonication. Shorter pulse lengths generally maintained a uniform cavitation activity throughout the pulse sequence. PRP=298kPa.

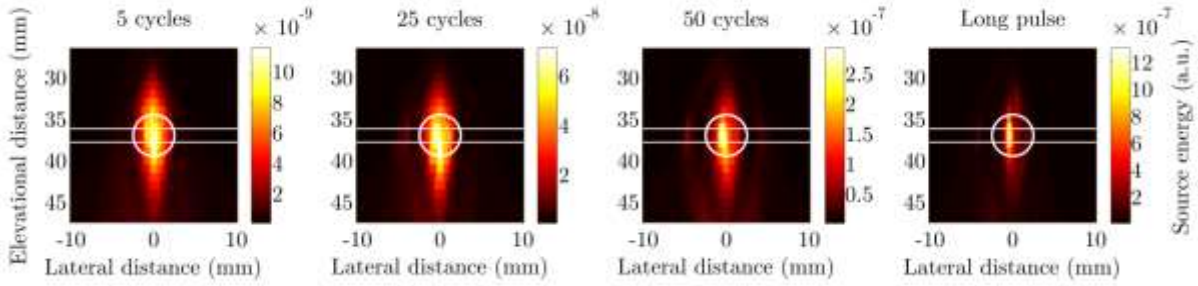


FIG.5. (Color online) Cumulative energy maps for 5, 25, 50 cycles, and long pulse. The upstream bias observed in the long pulse sonication at high pressures was greatly reduced at rapid short-pulse sonication, yielding a uniform cumulative energy distribution. PRP=603kPa.

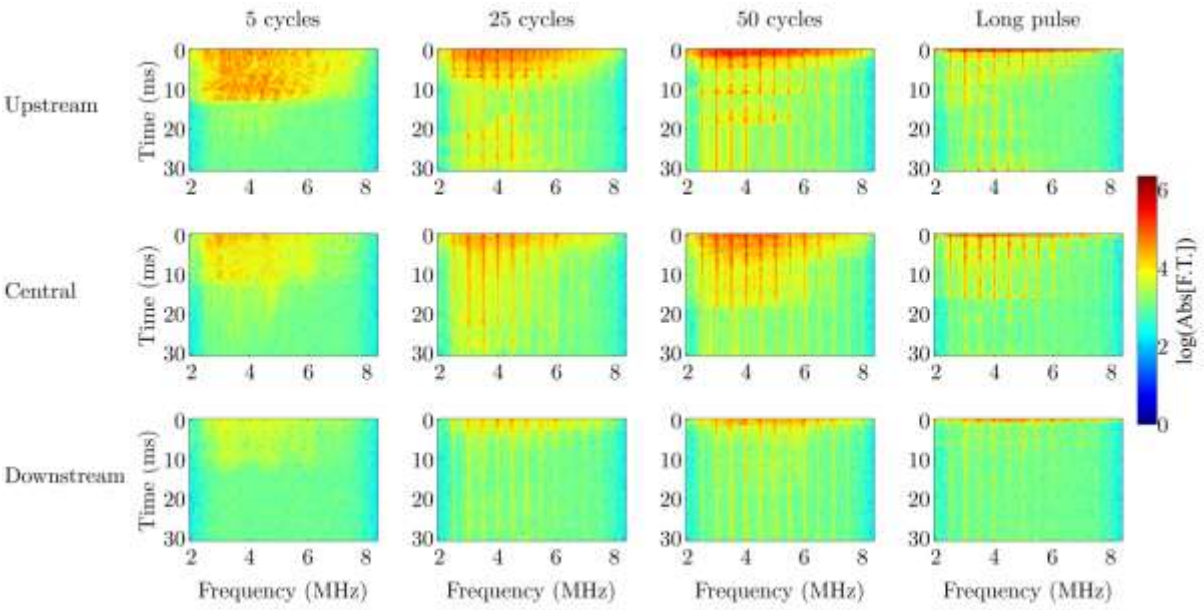


FIG. 6. (Color online) Spectrograms of the upstream (top), centre (centre) and downstream (bottom) points within the focus for different pulse lengths. High magnitude inertial cavitation at the central point indicated violent events leading to transient behaviours and microbubble destruction. Destruction rates at the center of the focus were higher for longer pulse lengths. Recurrent inertial cavitation was observed at the upstream point during the entire sonication duration, suggesting a continuous modification/destruction of microbubbles entering the focal volume. Lower magnitude stable cavitation dominated at the downstream point for all the tested sequences. PRP=298kPa.

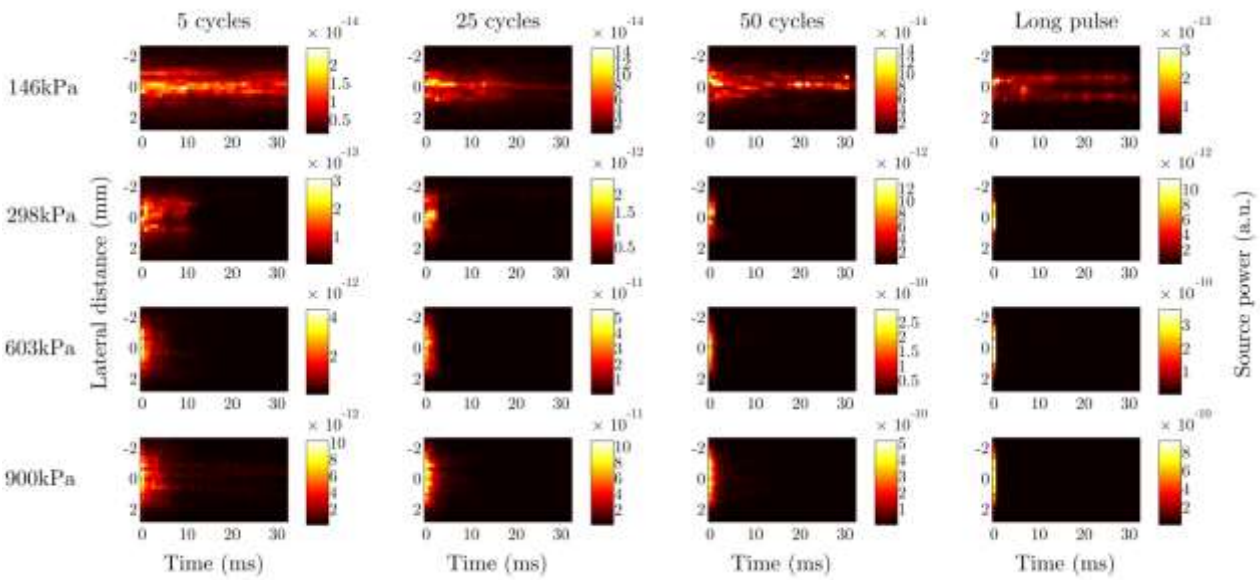


FIG. 7. (Color online) Lateral source power profiles over time for different pulse sequences (from left to right, PL: 5, 25, 50 and 16,667 cycles) at various sonication pressures (from top to bottom, PRP: 146, 298, 603 and 900kPa). Rapid short-pulse sequences produced a more uniform lateral distribution of acoustic cavitation activity over time and space when compared to the long pulse control, which maintained the activity only for a few ms.

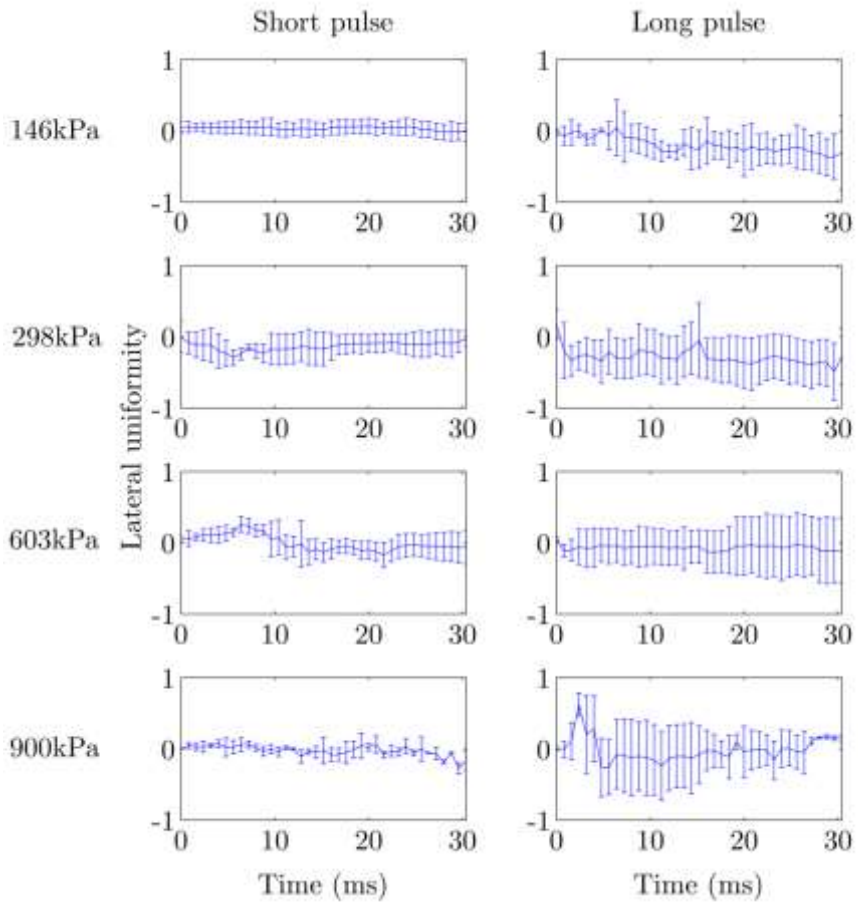


FIG. 8. (Color online) Lateral uniformity index for short-pulse (left, PL: 5 cycles) and long-pulse (right) sonication for the different acoustic pressures (from top to bottom, PRP: 146kPa, 298kPa, 603kPa, 900kPa). The lateral uniformity index ( $LU$ ) initially had values around 0 but over time shifted towards negative values for the long pulse sonication, indicating a shift from lateral uniformity to upstream bias and non-uniform distribution. In contrast, rapid short-pulse sequences generally maintained a uniform lateral distribution throughout the sonication duration. Averaging was performed across n=3 repetitions.

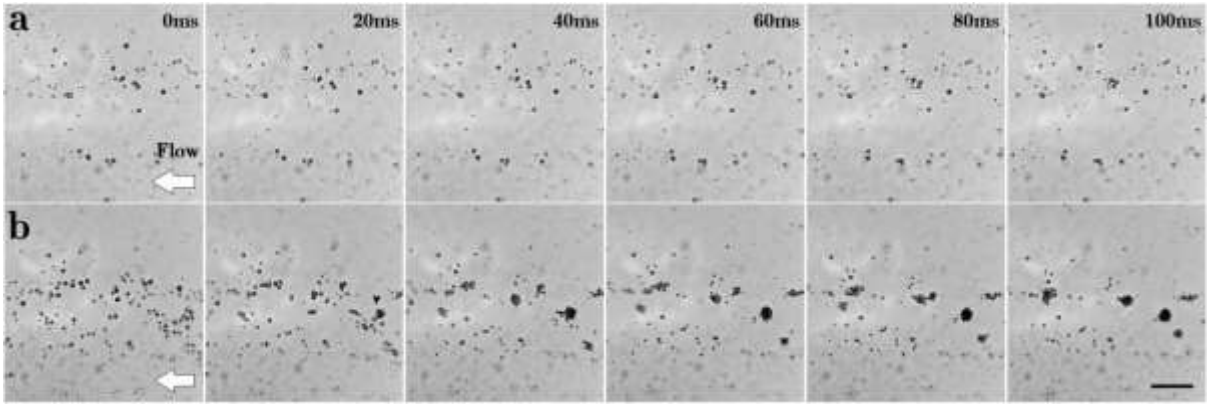


FIG. 9. Optical observations of microbubble dynamics during rapid short-pulse and low-power sonication at a) PRF=0.62kHz, and b) PRF=5kHz. High duty cycle sonication enhanced the effects of secondary radiation forces, producing microbubble clusters within the first 40ms. In contrast, low duty cycle sonication enhanced the mobility of the cavitation nuclei, which moved under the influence of the fluid drag force during the off-time of the rapid short-pulse sequence. The field-of-view was within the focal volume of the focused ultrasound transducer. PRP: 150kPa, PL: 25 cycles, flow speed=10mm/s from right to left. Bar: 50μm.